ACS SENSORS

pubs.acs.org/acssensors Article

Ultrasensitive Detection of Exosomes Using an Optical Microfiber Decorated with Plasmonic $MoSe_2$-Supported Gold Nanorod Nanointerfaces

Hongtao Li,* Tianqi Huang, Liang Lu, Hao Yuan, Lei Zhang, Hongzhi Wang,* and Benli Yu

Cite This: *ACS Sens.* 2022, 7, 1926−1935 Read Online

ACCESS | Metrics & More | Article Recommendations | Supporting Information

Downloaded via TSINGHUA UNIV on November 5, 2022 at 10:41:13 (UTC).
See https://pubs.acs.org/sharingguidelines for options on how to legitimately share published articles.

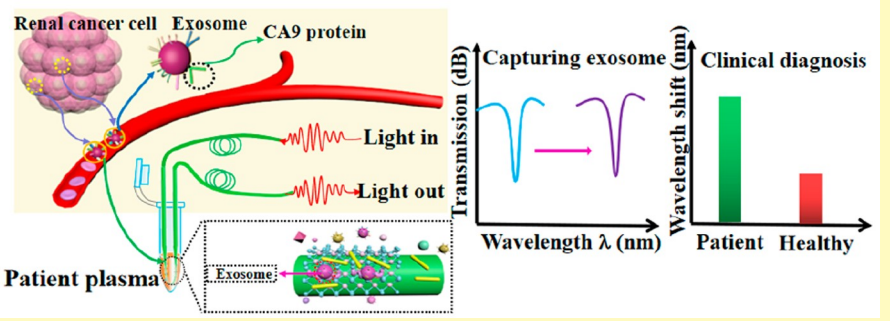

ABSTRACT: Exosomes are potential and promising natural noninvasive biomarkers for liquid biopsies and can be involved in various biological and pathological processes in early-stage cancer. Thus, there is an urgent demand to develop low-cost, small-size, remarkable-specificity, and ultrasensitive exosome biosensors for early clinical point-of-care (POC) testing. Although various conventional tumor exosome detection methods have been generally proposed, the low detection sensitivity and specificity significantly hinder their use in cancer clinical diagnosis and prognosis. To address the above challenges, an optical microfiber integrated with $MoSe_2$-supported gold nanorods is proposed. To tune the strong localized surface plasmon resonance (LSPR) of the nanointerfaces on the optical microfiber to be in accordance with the operating wavelength of the silica optical microfiber in the telecommunication band, gold nanorods with a high aspect ratio of approximately 10:1 are proposed. Due to the interaction between the excited LSPR effect and the evanescent field of the optical microfiber, the sensor can detect clear cell renal cancer exosomes within a wide concentration range from 10^0 particles/mL to 10^8 particles/mL, with an extremely low limit of detection (LOD) of 9.32 particles/mL, which is lower than that of current various state of the art methods. More importantly, the microfiber with high specificity can successfully differentiate pathological plasma and healthy controls, exhibiting very promising clinical applications in renal cancer diagnosis and prognosis. This work opens up a new approach for the *in situ* detection and quantification of exosomes with ultrahigh sensitivity in early clinical screening and diagnosis.

KEYWORDS: *clear cell renal cancer exosomes, optical microfiber biosensor, LSPR, CA9 protein, evanescent field, ultralow LOD*

With the development of diagnostic medicine for liquid biopsies, the rapid and precise detection of early-stage diseases calls for low-cost and portable biosensing probes for the ultrasensitive detection of new specific and credible biomarkers in bodily fluids, such as extracellular vesicles (EVs), circulating tumor cells (CTCs), and circulating tumor DNA (ctDNA).[1−4] Exosomes, as emerging promising and potential biomarkers, are subtypes of EVs, and they are within a diameter range of 30−150 nm.[5] Exosomes are secreted from the outward blebbing of the cellular membrane into various physiological fluids.[6,7] In addition, exosomes are enriched with many biological substances, including nucleic acids and membrane proteins, and they can carry these activated biomolecules from parental cells to recipient cells, which are involved in biological and pathological processes.[8,9] In recent years, the fact that tumor-derived exosomes can carry various endogenous cargos and reflect the pathophysiological condition has been of great interest, which makes them potential biomarkers for early-stage cancer.[10,11] However, the contents of exosomes in bodily fluids are extremely low in early-stage diagnostics. Thus, developing new biosensors for an ultrasensitive and specific-precision quantitative analysis of tumor-derived exosomes is imperative. Although some conventional techniques for the detection of exosomes have been reported,

Received: March 21, 2022
Accepted: June 16, 2022
Published: June 27, 2022

ACS Publications © 2022 American Chemical Society

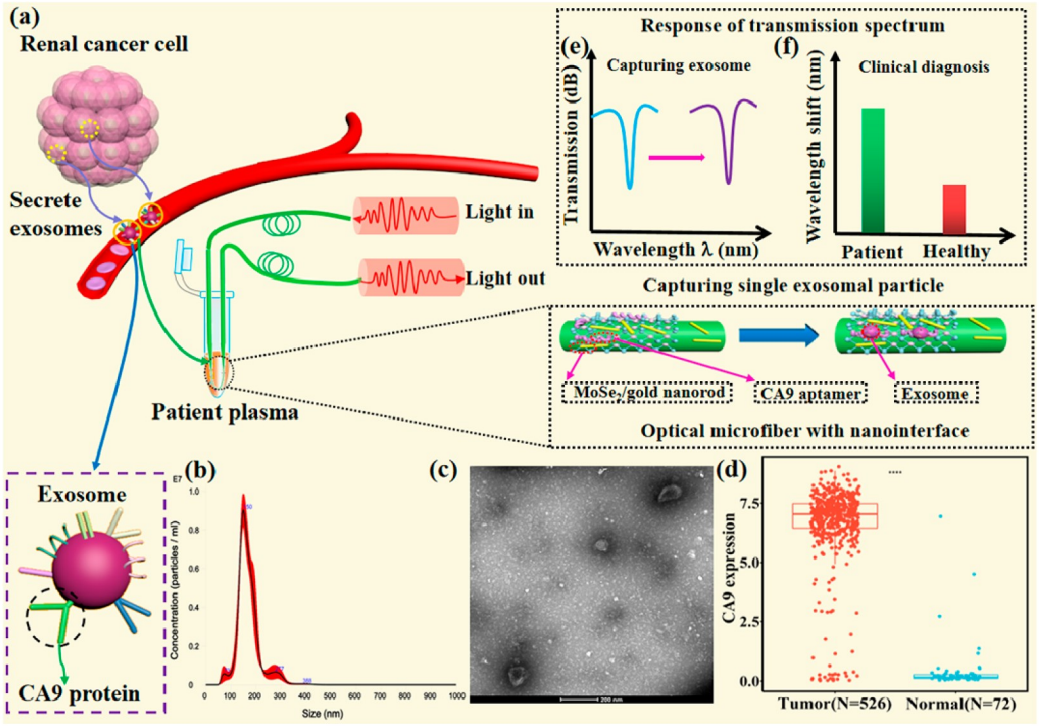

Figure 1. (a) Schematic of the detection process using an optical microfiber with $MoSe_2$-supported gold nanorods and CA9 aptamers. (b) Measured particle size of the exosomes. (c) SEM image of the exosomes in the experiments. (d) Screening of the specific CA9 protein expression in tumor patients and normal persons. (e) Exosome capture inducing a transmission spectral shift in the interferometric fringe. (f) Different optical signal responses with the sensor dipped into patient and healthy samples.

such as enzyme-linked immunosorbent assays (ELISAs),[12] Western blots,[13] the polymerase chain reaction (PCR),[14] and ultracentrifugation,[15] these methods suffer from complicated and time-consuming operating procedures, expensive equipment, low isolation efficiency, low sensing sensitivity, and excessive sample consumption.[16] To address the above issues, surface-enhanced Raman scattering (SERS),[17−19] colorimetric methods,[20,21] fluorescent methods,[22−26] surface plasmon resonance (SPR),[27,28] electrochemical methods,[29−33] and pH test paper method[34] have been extensively proposed for the highly sensitive detection of exosomes. Nevertheless, these methods are also confronted with the dire issues of being subjected to electromagnetic interference (electrochemical methods), tedious and complicated preprocessing nanoparticle probe preparation (SERS, fluorescent, and SPR methods), relatively low detection accuracy (colorimetric methods and pH test paper method), overdependence on an accurate operation involving technical skills, lack of continuous on-site real-time label-free detection (fluorescent methods), and low sensing sensitivity. Therefore, exploring a simple-structure, portable, ultrasensitive, remarkably specific, and easy-to-use biosensor for an *in situ* real-time quantitative analysis of tumor-derived exosomes is an urgent objective. As a recently developed alternative biosensing device, a silica optical microfiber can transduce interfacial refractive index (RI) variations into an optical signal response, and it possesses the great merits of low cost, millimeter length, lightweight, portability, immunity to electromagnetic fields, label-free nature, and flexible mechanical properties.[35−38] However, silica microfibers usually detect target biological solutions with limits of detection (LOD) as high as the picomolar or even nanomolar level, which strongly restricts their use in very early stage clinical diagnosis.[39,40] Because the small RI change of the microfiber is induced by the interaction between molecular binding on the fiber surface and the evanescent field, enhancing the evanescent field and thus improving the biosensing sensitivity is worthwhile. Recently, researchers found that plasmonic nanomaterials coupled with 2D materials on the fiber surface can efficiently improve the sensing sensitivity of optical microfibers,[41−46] including an optical microfiber with silver-nanoparticle-decorated graphene, which was fabricated for the detection of cytochrome *c*, with a LOD of 68.20 aM.[45] Furthermore, an optical microfiber was functionalized with black-phosphorus-supported Au nanohybrids for the detection of epidermal growth factor receptor (ErbB2), with a LOD of 6.72 zM, enabling detection at the single-molecule level.[46] Although the localized SPR (LSPR) was tuned to be consistent with the operating wavelength of the microfiber transducer within the telecommunication band,[46,47] the synthesized nanointerfaces on the microfiber entailed complicated constituents and time-consuming processing procedures.

Herein, we have developed an optical microfiber with $MoSe_2$ nanosheets to support high-aspect-ratio gold nanorods for the detection of clear cell renal cancer exosomes. The plasmon resonances of gold nanorods were tuned to the communication window, and high-aspect-ratio gold nanorods were synthesized via a simple seed-mediated growth method. In comparison to other two-dimensional (2D) transition-metal dichalcogenides (TMDCs) and graphene, $MoSe_2$ has a greater layer spacing with a smaller energy band gap and greater optical absorption efficiency, which can lead to it possessing excellent biosensing performance.[48−50] With the sensing performance enhancement due to the nanointerfaces, the microfiber sensor provides an

https://doi.org/10.1021/acssensors.2c00598
ACS Sens. 2022, 7, 1926−1935

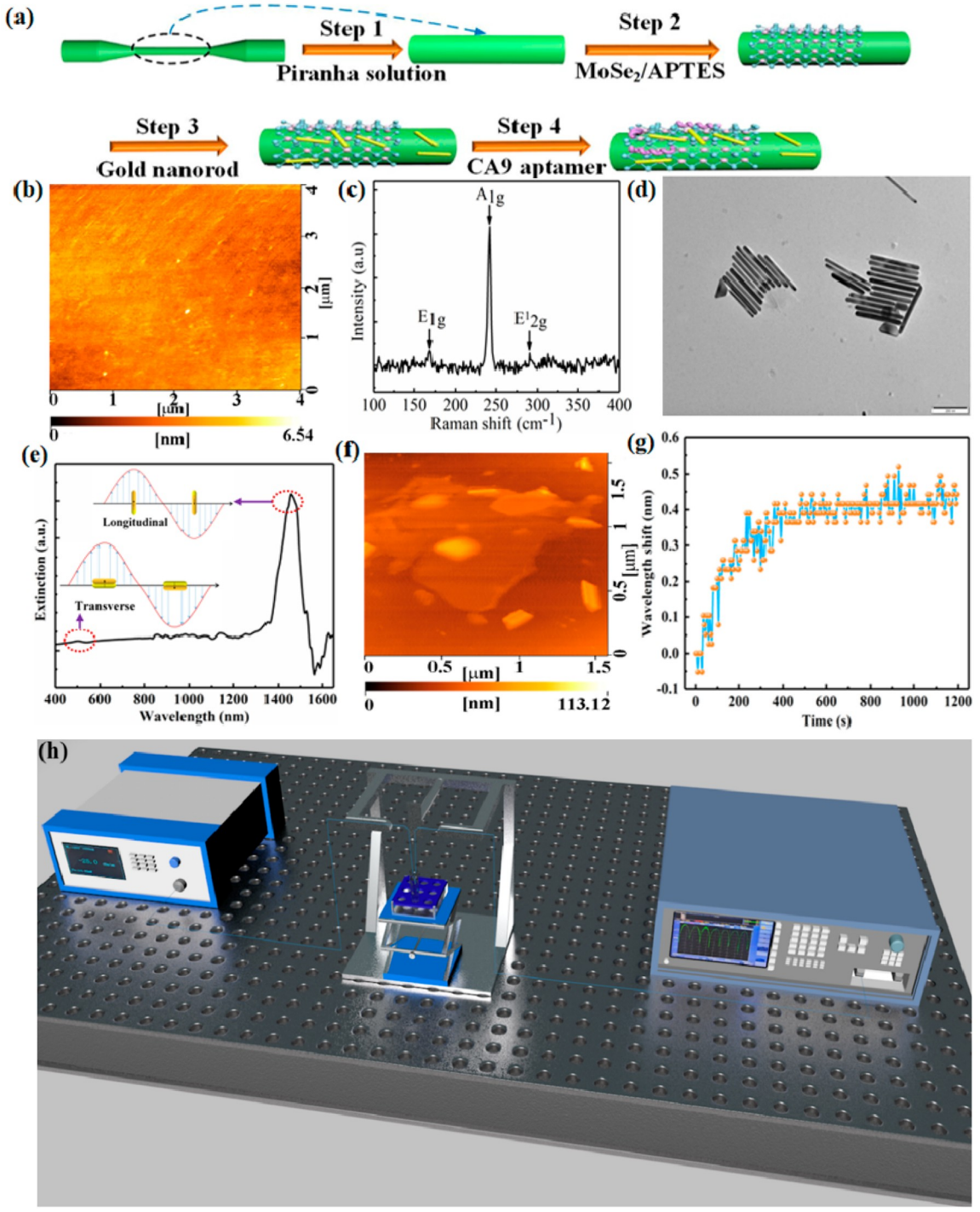

Figure 2. (a) Schematic diagram of the interfacial functionalization of the microfiber exosome biosensor. (b) AFM image of the pure silica microfiber surface. (c) Raman spectrum of the few-layer $MoSe_2$ nanosheets on the microfiber. (d) TEM image of gold nanorods with high aspect ratios. (e) Extinction spectrum of the gold nanorods. (f) AFM image of the microfiber with a $MoSe_2$ spacer and gold nanorods. (g) Process of CA9 aptamer immobilization on the optical microfiber probe. (h) Schematic diagram of the experimental setup for real-time *in situ* monitoring of the exosomes.

ultrahigh sensitivity for detecting exosomes, with an ultralow LOD of 9.32 particles/mL, which is lower than those of reported cutting-edge methods.[19,21,27,29] The microfiber is capable of differentiating clinical pathological plasma and healthy controls. This work opens up a novel method for the *in situ* detection and quantification of exosomes with ultrahigh sensitivity in early clinical screening and diagnosis.

RESULTS AND DISCUSSION

Principle of Clear Cell Renal Cancer Exosome Sensing. As a valuable intercellular communication vehicle in clear cell renal cancer, exosomes play very important roles in renal cancer pathological progression. Exosomes are derived from invagination of the renal cancer cell plasma membrane, and they can be released from the membrane into the

https://doi.org/10.1021/acssensors.2c00598
ACS Sens. 2022, 7, 1926−1935

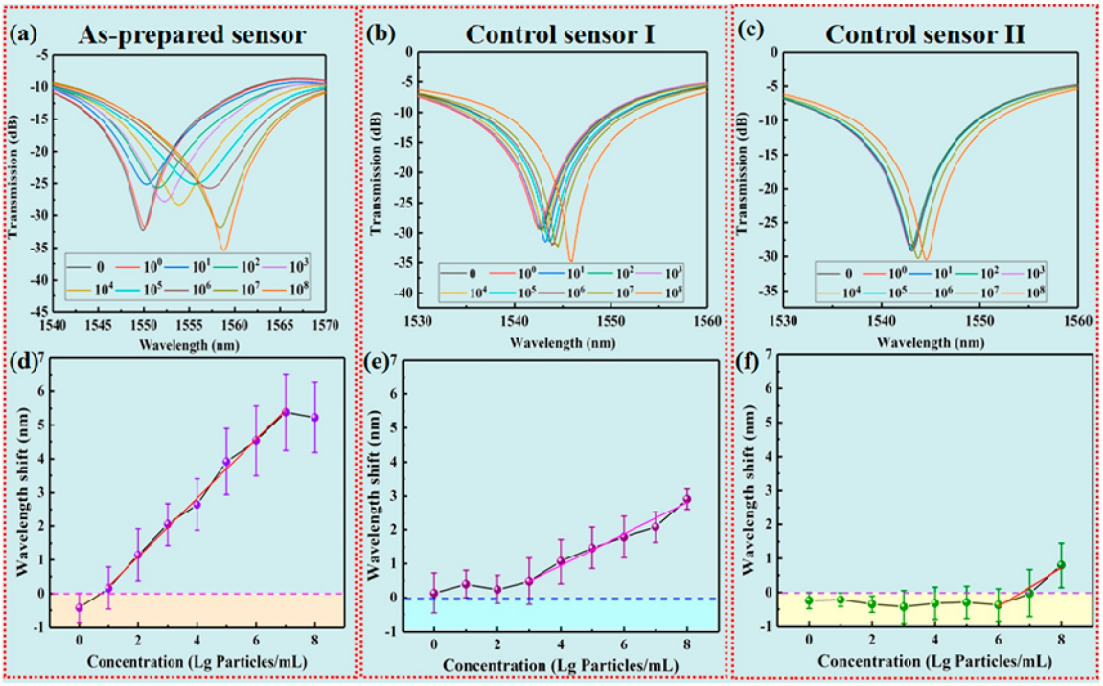

Figure 3. (a–c) Measured optical transmission spectra of an as-prepared microfiber sensor and two other control microfiber sensors as a function of exosome solution concentration. (d–f) Wavelength shifts of the as-prepared sensor and control sensors as a function of the exosome solution concentration. (a) and (d) are for the optical microfiber decorated with $MoSe_2$-supported gold nanorods and CA9 aptamers, (b) and (e) are for the sensor with gold nanorods and CA9 aptamers, and (c) and (f) are for the microfiber sensor only decorated with CA9 aptamers without any sensitized nanointerface. Error bars represent 1 standard deviation (n = 3).

extracellular microenvironment via exocytosis. In addition, renal cancer exosome particles are enriched with some membrane proteins (e.g., CA9 protein), miRNAs, DNA, nuclear proteins, etc. (Figure 1a). By using a nanoparticle tracking technique, we found that a majority of exosomes are 150 nm in size, and the results are shown in Figure 1b. Via scanning electron microscopy (SEM), we observed the detailed morphology of the exosomes, as shown in Figure 1c. Figure 1d shows the differences in specific protein expression between cancer patients and normal persons. Clearly, the CA9 protein is highly expressed in clear cell renal cancer for the majority of patients; in contrast, the protein is expressed at low levels in most normal persons. Therefore, the CA9 protein is regarded as an ideal receptor for renal cancer exosome detection.[51] As shown in Figure 1a, a nanointerface-sensitized optical microfiber with the specific probe of the CA9 aptamer is immersed in a renal cancer patient plasma sample. After the exosome particle enters the evanescent field of the microfiber, the CA9 aptamer on the microfiber can capture the target exosome in a curling manner. Under this circumstance, the refractive index (RI) on the surface of the microfiber is increased, and the variation information can be translated into a red shift in the transmission interferometric spectrum (Figure 1e). As depicted in Figure 1f, the patient plasma can induce a dynamic optical signal response, which is reflected in a larger wavelength red shift in the optical transmission spectrum.

Interfacial Functionalization of the Microfiber with $MoSe_2$-Supported Gold Nanorod Nanointerfaces. As presented in this paper, we fabricated an optical microfiber biosensor by using the flame-brushing technique, which is illustrated in Figure S1. Specifically, a silica thin-core fiber with a 1.80 μm core and a 125 μm cladding was slowly heated and stretched into a microsized optical microfiber. An image of the entire optical microfiber obtained through optical microscopy is shown in Figure S2a. According to the detailed observation of a fraction of the microfiber, the diameter of the microfiber was 11.44 μm, and the length of the uniform region was 2.40 mm. The results obtained above are shown in Figure S2b. Our fabricated optical microfiber functions as a Mach–Zehnder interferometer (MZI); the interference fringe in air is illustrated in Figure S2c. As an MZI, the high-order-mode HE_{12} can be excited from the transition region and can interfere with the intrinsic HE_{11} mode within the uniform region of the microfiber. Figure S3 shows the modal distributions of the HE_{11} and HE_{12} modes. As shown in Figure S3, the HE_{11} mode is confined inside the fiber, while the HE_{12} mode leaks out of the microfiber and is more sensitive to small variations in the external environment. Eventually, the effective indices of the two modes can be modulated, and the interference fringe of the microfiber MZI can be varied.

The design of the interfacial functionalization of the microfiber with $MoSe_2$–gold nanorod nanointerfaces and the CA9 aptamer is depicted in Figure 2a. The interface of the silica microfiber was sequentially modified by using piranha solution. An atomic force microscope (AFM) image shows that the surface of the silica microfiber was smoothly cleaned (Figure 2b).

A 3-aminopropyltriethoxysilane (APTES) solution was mixed with the $MoSe_2$ nanosheet dispersion solution, and the $MoSe_2$ nanosheets were endowed with positive charges. Subsequently, $MoSe_2$ nanosheets were immobilized on the microfiber interface due to a covalent reaction. As can be seen from Figure S4, $MoSe_2$ nanosheets were successfully immobilized on the microfiber surface, and the thickness of the nanosheets was approximately 5 nm. As shown in Figure S5a, we observed a dynamic wavelength red shift in the optical

https://doi.org/10.1021/acssensors.2c00598
ACS Sens. 2022, 7, 1926–1935

spectrum with a maximum value of 15 nm within 20 min. Figure 2c exhibits the measured Raman spectra of the $MoSe_2$ nanosheets. As shown in Figure 2c, three characteristic peaks of E_{1g} (168.92 cm^{-1}), A_{1g} (242.29 cm^{-1}) and $^1E_{2g}$ (290.43 cm^{-1}) were obtained, which coincided well with the locations of the peaks in the reported literature.[52−54] The morphology of the gold nanorods is presented in Figure 2d, obtained through transmission electron microscopy (TEM). According to the TEM image, the longitudinal length and transverse length of the gold nanorods were approximately 200 and 20 nm, respectively. To investigate the extinction property of the gold nanorods, we measured the two characteristic LSPR peaks located at 503 and 1456 nm corresponding to the transverse length and longitudinal length of the gold nanorods, respectively, in the ultraviolet−visible−near-infrared (UV−VIS−NIR) spectra, as shown in Figure 2e. Afterward, high-aspect-ratio gold nanorods decorated with carboxyl-polyethylene-mercapto (COOH-PEG-SH) could be successfully immobilized on the microfiber surface through a dehydration−condensation reaction. Figure S5b depicts the wavelength shift as a function of time with the gold nanorods immobilized on the microfiber surface. Due to the negative group index of gold nanorods, a blue shift in the optical spectrum occurred, with a maximum wavelength shift of −0.40 nm within 20 min. Figure 2f presents an AFM image of the microfiber interface functionalized by $MoSe_2$-supported gold nanorods. One can see in Figure 2f that nanointerfaces were successfully bonded on the surface of the microfiber. Eventually, the proposed microfiber could successfully capture CA9 aptamers via an electrostatic attraction, which could be reflected in the gradual red shift in the transmission spectrum with increasing reaction time, as shown in Figure 2g. Figure 2h illustrates the experimental setup for clear cell renal cancer exosome sensing. As demonstrated in Figure 2h, the as-prepared microfiber was immersed in the target aqueous solutions with a total volume of 1 mL, a broad-band source (BBS) provided incident light within the spectral range of 1250−1650 nm, and an optical spectrum analyzer (OSA) with a minimum resolution of 0.02 nm was employed to monitor *in situ* the real-time biological reactions.

Clear Cell Renal Cancer Exosome Sensing. The exosome sensing abilities of the as-prepared microfiber sensor and control sensors I and II are shown in Figure 3. In our experiments, the nanointerfaces of the as-prepared optical microfiber sensor with CA9 aptamers consisted of $MoSe_2$-supported gold nanorods, while those of control microfiber sensors I and II with CA9 aptamers consisted of gold nanorods and materials without any nanointerface sensitization, respectively. The above three microfiber sensors were obtained from the same optical microfiber device with a diameter of 11.44 μm. Before exosome sensing, the three sensors were separately dipped into phosphate-buffered saline (PBS) solutions for 1 h to reduce the interference of the nonspecific ions in PBS during the biosensing measurements.[44] Figure S6 illustrates the stability of the three sensors in pure PBS solutions. According to a numerical analysis, the three standard deviations s_1 (as-prepared sensor), s_2 (control sensor I) and s_3 (control sensor II) were 0.01, 0.02, and 0.04, respectively. To investigate the sensing abilities of the three sensors, the sensors were all immersed into exosome solutions with different concentrations ranging from 10^0 particles/mL to 10^8 particles/mL. When the as-prepared sensor was exposed to the solutions, obvious and regular red shifts of wavelength dips occurred, which is demonstrated in Figure 3a. The as-prepared sensor exhibited a wide linear response with a high sensing sensitivity of 0.87 nm per log particles/mL and a perfect linearity of 99.40% within the exosome concentration range of 10^0−10^8 particles/mL, as shown in Figure 3d. On the basis of the given s_1 value and the sensitivity, one can obtain the LOD of the sensor using the equation[55]

$$x_{LOD} = f^{-1}(\overline{y_{black}} + 3\sigma) \quad (1)$$

where f^{-1} indicates the inverse of the fitting function and $\overline{y_{black}}$ denotes the average value of the wavelength shift in the linear response region for the exosome concentration. For the as-prepared sensor, $\overline{y_{black}}$ equals 0.16 nm. Finally, we calculated that the LOD of the sensor was 9.32 particles/mL, which is lower than those of reported cutting-edge methods.[19,21,27,29]

The specific nanointerfaces of control sensor I were composed of gold nanorods and CA9 aptamers, as depicted in Figure S7a. The wavelength variation −0.20 nm of the sensor during the functionalization process is presented in Figure S7b. Aptamers were successfully anchored on the microfiber surface via a covalent reaction, and the maximum wavelength variation was approximately 0.10 nm, as shown in Figure S7c. By calculating eq 1, the detection sensitivity and $\overline{y_{black}}$ of control sensor I were 0.47 per log particles/mL and 0.48 nm, respectively, with a linearity of 96.10% (Figure 3b,e). The LOD of sensor I was calculated as 1.37×10^3 particles/mL. For control sensor II, the detection sensitivity and $\overline{y_{black}}$ were 0.57 per log particles/mL and −0.37 nm, respectively (Figure 3c,f). A relatively high LOD of 1.96×10^6 particles/mL was obtained for the sensor.

Figure S8 demonstrates the sensing abilities of the as-prepared sensor and other control I and II sensors in exosome solutions with a unit concentration of 10^2 particles/mL. Obviously, the as-prepared microfiber sensor could successfully detect the exosomes in solution at this ultralow concentration, in which the very few exosome molecules could induce a red shift of ∼0.20 nm for the transmission dip (Figure S8a). Due to the lack of $MoSe_2$-supported gold nanorod nanointerfaces, control sensors I and II could not sense the target component at such a low concentration (Figure S8b and c).

As described above, the $MoSe_2$-supported gold nanorod nanointerfaces could greatly improve the sensing ability of the optical microfiber in the detection of exosomes at ultralow concentrations.

Specificity of the As-Prepared Exosome Sensor. In the real extracellular physiological environments of human beings, some complicated interfering ions, inorganics, and organics exist. To meet the demands of clinical assays and diagnosis, the sensor must be able to specifically differentiate the target object from the complicated extracellular environment. To mimic the real physiological environment of extracellular body fluids, target particles of clear cell renal cancer exosomes with a relatively low concentration of 10^4 particles/mL and some interfering control analytes (i.e., Na^+, K^+, glucose, urea, human serum albumin (HSA), and fibrinogen gamma chain (FGG) with ultrahigh concentrations of 10^{-6} mol/L) were chosen, as indicated in Figure 4. As demonstrated in Figure 4, only the exosomes could cause a dynamic transmission wavelength variation of 2.64 nm, while the other interfering analytes could not induce a notable optical signal response according to separate detections of each solution using our as-prepared exosome sensor. In addition, when the exosome solution with a

https://doi.org/10.1021/acssensors.2c00598
ACS Sens. 2022, 7, 1926−1935

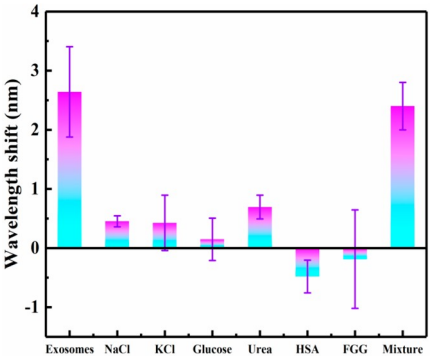

Figure 4. Comparison of the as-prepared optical microfiber biosensor responses to pure exosome solution with a concentration of 10^4 particles/mL, other interfering analytes with a high concentration of 10^6 M, and a solution mixture consisting of the exosome solution (10^4 particles/mL) and all interfering components (10^6 M). Error bars represent 1 standard deviation (n = 3).

concentration of 10^4 particles/mL was mixed with the other control analyte solutions, a significant wavelength shift of 2.40 nm still occurred, which was attributed to the existence of exosome molecules. The energy loss of the as-prepared microfiber sensor immersed into the solution mixture was why the induced wavelength shift in the mixture solution was smaller than that in the pure exosome solution.[56] Thus, the proposed microfiber exosome sensor with such remarkable specificity is promising for effectively conducting *in situ* sensing of clinical samples.

It is necessary to directly verify the exosome capture by the CA9 aptamer on the microfiber. To this end, we have added an AFM image on the optical microfiber sensor coated with exosomes after sensing the sample in PBS solution in Figure S9a. According to the AFM image, it was observed that the surface roughness and thickness of microfiber increased obviously after capturing the exosomes, when the AFM images in Figure 2b,f are compared. Figure S9b shows the SEM image on the optical microfiber sensor coated with exosomes after sensing the sample in PBS solution. It was obvious that the exosomes with a diameter of about 150 nm were randomly distributed on the optical microfiber surface.

Real Plasma Sample Analysis of Exosomes for Cancer Diagnosis. As a noninvasive biosensing tool, the capability of the as-prepared optical microfiber exosome sensor to detect and assay renal cancer patient plasma and healthy plasma for renal cancer diagnosis was assessed and evaluated, as shown in Figure 5. The microfiber sensor with a compact size could be used to sense the plasma samples collected from clear cell renal cancer patients (n = 10) and healthy controls (n = 5). On the basis of quantification of the contents of the exosomes in the two types of plasma samples, the renal cancer patient plasma samples could all induce an evident spectral response, indicating that the renal cancer exosome particles were caught through binding of the high-expression CA9 protein on the exosome surface to the aptamers on the as-prepared microfiber sensor in the plasma samples, as recorded in Figure 5a and Figure S10a. As shown in Figure 5b and Figure S10b, the healthy plasma samples could also cause an optical response to a certain extent, which was a result of the low expression of CA9 protein on the exosome surface in the healthy plasma samples. In order to confirm whether the exosomes in the renal cancer patients' plasma used in this study express CA9, it is necessary to directly observe CA9-mediated exosome capture on the optical microfiber surface in the patent's sample. To this end, we have obtained an AFM image of the CA9-mediated exosome capture on the optical microfiber in a renal cancer patient's plasma, as shown in Figure S10c. In Figure S10c, the surface roughness increased very obviously after capturing exosomes in a renal cancer patient's plasma. This is the reason that CA9 protein is highly expressed on the exosome surface for a clear cell renal cancer patient. Thus, our proposed as-prepared microfiber sensor with ultrahigh sensitivity and outstanding specificity could differentiate pathological plasma and healthy controls. These assay results demonstrate a new exosome diagnostic approach for liquid biopsy and pave the way for applications in very early stage clinical screening, diagnosis, and prognosis.

LSPR Enhancement of the As-Prepared Optical Microfiber. For this RI sensor, the evanescent field of the optical microfiber plays an extremely important role in sensing the small RI variations of the fiber interface. By employing the commercial software COMSOL Multiphysics, we simulated the modal distribution of the microfiber with a diameter of 11.44 μm (Figure S3). The simulation results show that the

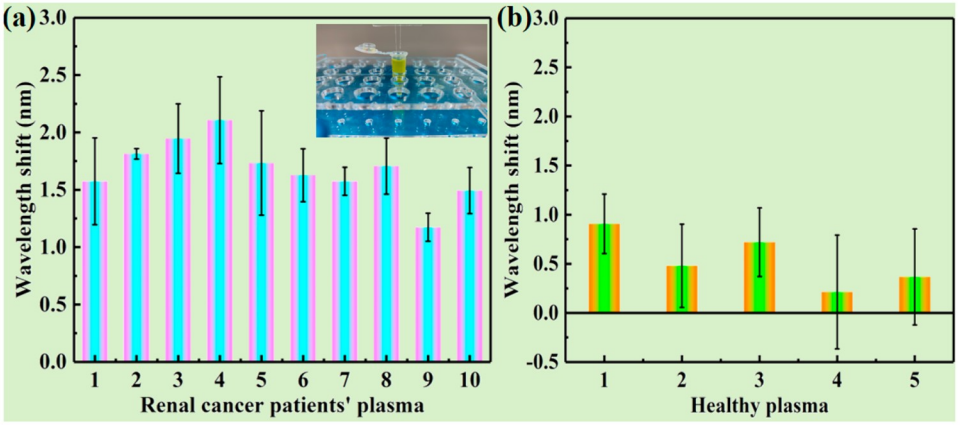

Figure 5. (a) Optical response of the sensor to renal cancer patient plasma. (b) Optical response of the sensor to healthy plasma. Clinical samples were collected from clear cell renal cancer patients (n = 10) and healthy controls (n = 5). Error bars represent 1 standard deviation (n = 3) Inset in (a): Photo of microfiber sensing in plasma.

https://doi.org/10.1021/acssensors.2c00598
ACS Sens. 2022, 7, 1926−1935

energy of the evanescent field is mainly contributed by the high-order mode HE_{12}. By an analysis of the simulation data, the penetration depth of the evanescent wave for the HE_{12} mode is 2.47 μm, as displayed in Figure S11. Therefore, the strong enhancement of the energy density of the HE_{12} mode within the evanescent field can effectively improve the sensing sensitivity. In this model, the intensity of the HE_{12} mode is positively correlated with the microfiber propagation constant. The induced variation in the propagation constant is determined by the formula[57]

$$\frac{\Delta\beta}{\beta} \cong -\frac{mk|E(x,y)|^2 V_0}{\int L\cdot|E(l)|^2 \, dS} \quad (2)$$

where m depicts the quantity of binding exosomes, k denotes a constant determined by the permittivity of the exosomes, $E(x,y)$ indicates the intensity of the local electric at the exosome binding site, V_0 is the volume of a single exosome, L represents the uniform waist length of the proposed optical microfiber, $E(l)$ is the electric field, and S is the space of the microfiber sensing surface. For a given microfiber device and category of target molecules, the parameters m, k, V_0, L, $E(l)$, and S are certain. Therefore, improving the local electric field at the exosome binding site can greatly enhance the sensing sensitivity. To investigate the local electric field of the $MoSe_2$-supported gold nanorod nanointerfaces on the microfiber, we numerically investigated the three different types of nanointerfaces on the microfiber surface by using a finite-difference time-domain (FDTD) approach, and the regions of interest of the nanointerfaces were excerpted from parts of SEM images (Figure S12a,c). The measured AFM and TEM images show that the thickness of the $MoSe_2$ nanosheets was approximately 5 nm, and the transverse and longitudinal lengths of the gold nanorods were approximately 20 and 200 nm, respectively. The RI of $MoSe_2$ at a wavelength of 1550 nm was acquired from ref 58. By application of the obtained parameters, the numerical simulation results of the three nanointerfaces on the microfiber surface are displayed in Figure S12b,d–f. As shown in Figure S12f, the maximum $E(x,y)$ of the microfiber with $MoSe_2$-supported gold nanorods was 2.34-fold higher than that of the microfiber with only gold nanorods and 1104-fold higher than that of the microfiber without any nanointerface. As a consequence, the microfiber surface with $MoSe_2$-supported gold nanorods could induce a dynamic wavelength shift and realize an ultrahigh sensing sensitivity.

CONCLUSIONS

This work presented a microfiber MZI functionalized with $MoSe_2$-supported gold nanorods for the detection of clear cell renal cancer exosomes. The microfiber biosensor could sense a broad range of concentrations from 10^0 particles/mL to 10^8 particles/mL, with an extremely low LOD of 9.32 particles/mL. The LOD result is much lower than those of current various state of the art methods.[19,21,27,29] More importantly, the microfiber with high specificity can successfully differentiate pathological plasma and healthy controls, exhibiting very promising clinical applications. This work demonstrates a new exosome diagnostic approach for liquid biopsy and paves the way for applications in very early stage clinical screening, diagnosis, and prognosis.

MATERIALS AND METHODS

Materials. All chemical reagents were provided by the Sigma–Aldrich Reagent Database, Inc. They were of analytical grade and were used without further purification. PBS solution (pH 7.4) was supplied by Beijing Solarbio Science & Technology Co., Ltd. Tris(hydroxymethyl)aminomethane (Tris buffer, pH 7.4, 1.0 M) and the ssDNA (5′-COOH-AGCAGCACAGAGGTCAGATGTGG GCGCAGTGATGGGTTGGTCCTATGCGTGCTACCGTCCT ATGCGTGCTACCGTGAA-3′) aptamer were purchased from Sangon Inc. (Shanghai, China). The CA9 aptamer plays a very important role in sensing the clear cell renal cancer exosomes. CA9 aptamer is a single-stranded DNA strand, also named the CAIX aptamer, that bound to CAIX was sequenced by high-throughput sequencing in ref 59. According to ref 59, CA9 aptamer could specifically bind to the CA9-positive cells or other biomarkers. Therefore, the CA9 aptamer could specifically bind to CA9-positive clear cell renal cancer exosomes in this paper. FGG and HSA solutions were purchased from Sigo Biological Inc. (Beijing, China). The $MoSe_2$ nanosheet dispersion solution was synthesized and provided by Beike New Material Technology Co., Ltd. (Beijing, China). COOH-PEG-SH powder was supplied by Yuanye Bio-Technology Co., Ltd. (Shanghai, China). Exosome particles were extracted from clear cell renal cancer cells by H. Wang at the Department of Urology of the First Affiliated Hospital of Anhui Medical University. Clinical patient and healthy plasma samples were collected and provided by H. Wang from the First Affiliated Hospital of Anhui Medical University.

The exosome solution was diluted with PBS solution to concentrations from 10^8 particles/mL to 10^0 particles/mL. NaCl, KCl, glucose, and urea solutions were diluted with deionized (DI) water to concentrations of 10^{-6} mol/L. The HSA and FGG solutions were diluted with PBS to concentrations of 10^{-6} mol/L. Plasma samples were obtained by centrifuging the clinical whole blood samples.

Preparation of the Aminated $MoSe_2$ Nanosheet Dispersion Solution. The dispersion solution of $MoSe_2$ nanosheets was prepared by mixing them with APTES (99%) solution at a volume ratio of 1/2 and stirring for 1 h in a glovebox filled with nitrogen gas.

Synthesis and Functionalization of High-Aspect-Ratio Gold Nanorods. The seed solution was prepared by adding $NaBH_4$ solution with a concentration of 0.01 M into a mixture of CTAB solution (concentration of 0.20 M) with $HAuCl_4$ solution (concentration of 0.0005 M) and stirring for 2 min. Next, the above solution mixture was stored at room temperature for 2 h. Finally, 10 mL of the seed solution was added to the growth solution (consisting of CTAB with a volume of 4.50 mL, $HAuCl_4$ with a volume of 0.32 mL, and ascorbic acid with a volume of 0.10 mL).[60]

COOH-PEG-SH powder was dissolved in DI water with the help of ultrasonication and stirring for 1 h. Carboxylated gold nanorods were obtained by mixing the gold nanorod solution with a COOH-PEG-SH aqueous solution for 12 h.

Characterization. The surface morphologies of microfibers with different nanointerfaces were observed by AFM (5500M, Hitachi) and SEM (S-4800, Hitachi, Japan). The morphology of the gold nanorods was observed by HR-TEM (JEM-2100). The Raman spectra of the $MoSe_2$ nanosheets were measured by a Raman spectrometer (Renishaw inVia, excited by a 488 nm laser line). The extinction spectra of the gold nanorods were acquired with an UV–VIS–NIR spectrophotometer (PerkinElmer, Lambda 750S).

Fabrication of the Optical Microfiber Device. A flame-brushing technique was applied to fabricate the optical microfiber device based on an oxy-hydrogen flame tapering platform. Specifically, a silica thin-core single-mode fiber (UHNA3, Nufern Inc.) was heated by a flame and slowly drawn at a rate of 0.04 m/s. Notably, the hydrogen flow rate was controlled at 200 mL/min in this tapering process.

Experimental Setup. In the sensing system, incident light over a spectral bandwidth of 1250–1650 nm was launched from a BBS. The average light intensity of the BBS was approximately −30 dBm. An

https://doi.org/10.1021/acssensors.2c00598
ACS Sens. 2022, 7, 1926–1935

OSA with a minimum resolution of 0.02 nm was employed to monitor the transmission spectrum of the optical microfiber.

Sensing Mechanism. The fabricated optical microfiber is regarded as an MZI. Its detection mechanism can be represented by the differential equation

$$\frac{d\lambda}{dn_{sur}} = \frac{\lambda_{dip}}{\Gamma}\cdot\left(\frac{1}{\Delta n_{eff}}\cdot\frac{\partial \Delta n_{eff}}{\partial n_{sur}}\right) \quad (3)$$

where $\Gamma = 1 - \frac{\lambda_{dip}}{\Delta n_{eff}}\cdot\frac{d\Delta n_{eff}}{d\lambda}$ indicates the dispersion factor, which is normally negative for our fabricated microfiber. n_{sur} is the RI of the microfiber surface. l_{dip} represents the wavelength of a transmission dip. Δn_{eff} indicates the difference between the effective index of the HE_{11} mode and the effective index of the HE_{12} mode.

Numerical Simulations. The modal distributions and evanescent field profile of the optical microfiber were simulated and calculated by the commercial COMSOL Multiphysics software on the basis of the finite element method (FEM) at a wavelength of 1550 nm. Near-field mapping of the microfiber with different nanointerfaces was simulated by the FDTD method on the basis of the measured geometrical parameters of the $MoSe_2$ nanosheets and gold nanorods.

■ ASSOCIATED CONTENT

Supporting Information

The Supporting Information is available free of charge at https://pubs.acs.org/doi/10.1021/acssensors.2c00598.

Photograph of instruments for fabricating the optical microfiber, photograph and transmission spectrum of the fabricated whole optical microfiber configuration, simulation results of the modal distribution of the microfiber, AFM image of the optical microfiber functionalized with $MoSe_2$ nanosheets, wavelength shift as a function of time by using the as-prepared microfiber decorated with $MoSe_2$ nanosheets and gold nanorods, optical response as a function of time for three different types of optical microfibers immersed in pure PBS solution, AFM image of the optical microfiber surface decorated with pure gold nanorods, optical response versus time for the microfiber functionalized with gold nanorods, and wavelength shift as a function of time for the microfiber probe with CA9 aptamers, transmission spectral response of the three optical microfiber exosome sensors to the renal cancer exosome solution with an ultralow concentration of 10^2 particles/mL, experimental transmission spectral response with time obtained by immersing the as-prepared optical microfiber into a clear cell renal cancer patient plasma sample and a healthy plasma sample, simulated and calculated transverse electric field amplitude distributions of the high-order mode in the fiber, and SEM images and near-field mappings of different nanointerfaces on the optical microfiber (PDF)

■ AUTHOR INFORMATION

Corresponding Authors

Hongtao Li − *Information Materials and Intelligent Sensing Laboratory of Anhui Province and School of Physics and Optoelectronics Engineering, Key Laboratory of Optoelectronic Information Acquisition and Manipulation of Ministry of Education, Anhui University, Hefei 230601, People's Republic of China; Guangxi Key Laboratory of Nuclear Physics and Nuclear Technology, College of Physics Science and Technology, Guangxi Normal University, Guilin 541004, People's Republic of China;* orcid.org/0000-0001-5616-490X; Email: htli@ahu.edu.cn

Hongzhi Wang − *Department of Urology, The First Affiliated Hospital of Anhui Medical University, Hefei 230031, People's Republic of China; Institute of Urology, Anhui Medical University, Hefei 230031, People's Republic of China;* orcid.org/0000-0001-6813-0205; Email: wanghongzhi0830@163.com

Authors

Tianqi Huang − *Information Materials and Intelligent Sensing Laboratory of Anhui Province and School of Physics and Optoelectronics Engineering, Key Laboratory of Optoelectronic Information Acquisition and Manipulation of Ministry of Education, Anhui University, Hefei 230601, People's Republic of China*

Liang Lu − *Information Materials and Intelligent Sensing Laboratory of Anhui Province and School of Physics and Optoelectronics Engineering, Key Laboratory of Optoelectronic Information Acquisition and Manipulation of Ministry of Education, Anhui University, Hefei 230601, People's Republic of China*

Hao Yuan − *Information Materials and Intelligent Sensing Laboratory of Anhui Province and School of Physics and Optoelectronics Engineering, Key Laboratory of Optoelectronic Information Acquisition and Manipulation of Ministry of Education, Anhui University, Hefei 230601, People's Republic of China*

Lei Zhang − *Information Materials and Intelligent Sensing Laboratory of Anhui Province and School of Physics and Optoelectronics Engineering, Key Laboratory of Optoelectronic Information Acquisition and Manipulation of Ministry of Education, Anhui University, Hefei 230601, People's Republic of China*

Benli Yu − *Information Materials and Intelligent Sensing Laboratory of Anhui Province and School of Physics and Optoelectronics Engineering, Key Laboratory of Optoelectronic Information Acquisition and Manipulation of Ministry of Education, Anhui University, Hefei 230601, People's Republic of China*

Complete contact information is available at: https://pubs.acs.org/10.1021/acssensors.2c00598

Notes

The authors declare no competing financial interest.

■ ACKNOWLEDGMENTS

We acknowledge the support of the National Natural Science Foundation of China (Nos. 62105001 and 61741501), the Open Project of Guangxi Key Laboratory of Nuclear Physics and Nuclear Technology (No. NLK2021-11), the University Synergy Innovation Program of Anhui Province (No. GXXT-2020-050), and the Natural Science Foundation of Anhui province (Nos. 2108085MA19 and 2008085MF207). We thank the American Journal Experts for editing the manuscript for grammar, clarity, and consistency with a specific emphasis on improving the language of the text.

■ REFERENCES

(1) Haber, D. A.; Velculescu, V. E. Blood-based analyses of cancer: circulating tumor cells and circulating tumor DNA. *Cancer Discovery* **2014**, *4*, 650−661.

(2) He, M.; Zeng, Y. Microfuidic exosome analysis toward liquid biopsy for cancer. *J. Lab. Autom.* **2016**, *21*, 599−608.
(3) Im, H.; Shao, H.; Park, Y. L.; Peterson, V. N.; Castro, C. M.; Weissleder, R.; Lee, H. Label-free detection and molecular profiling of exosomes with a nano-plasmonic sensor. *Nat. Biotechnol.* **2014**, *32*, 490−495.
(4) Zhang, P.; Zhou, X.; He, M.; Shang, Y.; Tetlow, A. L.; Godwin, A. K.; Zeng, Y. Ultrasensitive detection of circulating exosomes with a 3D-nanopatterned microfluidic chip. *Nat. Biomed. Eng.* **2019**, *3*, 438−451.
(5) Kalluri, R. The biology and function of exosomes in cancer. *J. Clin Invest.* **2016**, *126*, 1208−1215.
(6) Kalluri, R.; LeBleu, V. S. The biology, function, and biomedical applications of exosomes. *Science* **2020**, *367*, eaau6977.
(7) Jiang, L.; Gu, Y.; Du, Y.; Liu, J. Exosomes: diagnostic biomarkers and therapeutic delivery vehicles for cancer. *Mol. Pharmaceutics* **2019**, *16*, 3333−3349.
(8) Valadi, H.; Ekstrom, K.; Bossios, A.; Sjostrand, M.; Lee, J. J.; Lotvall, J. O. Exosome-mediated transfer of mRNAs and microRNAs is a novel mechanism of genetic exchange between cells. *Nat. Cell Biol.* **2007**, *9*, 654−659.
(9) Zomer, A.; Maynard, C.; Verweij, F. J.; Kamermans, A.; Schafer, R.; Beerling, E.; Schiffelers, R. M.; de Wit, E.; Berenguer, J.; Ellenbroek, S. I. J.; Wurdinger, T.; Pegtel, D. M.; van Rheenen, J. In Vivo imaging reveals extracellular vesicle-mediated phenocopying of metastatic behavior. *Cell* **2015**, *161*, 1046−1057.
(10) Mohammadi, M.; Zargartalebi, H.; Salahandish, R.; Aburashed, R.; Wey Yong, K.; Sanati-Nezhad, A. Emerging technologies and commercial products in exosome-based cancer diagnosis and prognosis. *Biosens. Bioelectron.* **2021**, *183*, 113176.
(11) Kucharzewska, P.; Belting, M. Emerging roles of extracellular vesicles in the adaptive response of tumour cells to microenvironmental stress. *J. Extracell. Vesicles* **2013**, *2*, 20304.
(12) Lee, J.; Kim, H.; Heo, Y.; Yoo, Y. K.; Han, S. I.; Kim, C.; Hur, D.; Kim, H.; Kang, J. Y.; Lee, J. H. Enhanced paper-based ELISA for simultaneous EVs/exosome isolation and detection using streptavidin agarose-based immobilization. *Analyst* **2020**, *145*, 157−164.
(13) Kowal, E. J. K.; Ter-Ovanesyan, D.; Regev, A.; Church, G. M. Extracellular vesicle isolation and analysis by western blotting. *methods Mol. Biol.* **2017**, *1660*, 143−152.
(14) Lin, L. Y.; Yang, L.; Zeng, Q.; Wang, L.; Chen, M. L.; Zhao, Z. H.; Ye, G. D.; Luo, Q. C.; Lv, P. Y.; Guo, Q. W.; Li, B. A.; Cai, J. C.; Cai, W. Y. Tumor-originated exosomal lncUEGC1 as a circulating biomarker for early-stage gastric cancer. *Mol. Cancer.* **2018**, *17*, 84.
(15) Wei, R.; Zhao, L.; Kong, G.; Liu, X.; Zhu, S.; Zhang, S.; Min, L. Combination of Size-Exclusion Chromatography and Ultracentrifugation Improves the Proteomic Profiling of Plasma-Derived Small Extracellular Vesicles. *Biol. Proced. Online* **2020**, *22*, 12.
(16) Xiong, H.; Huang, Z.; Yang, Z.; Lin, Q.; Yang, B.; Fang, X.; Liu, B.; Chen, H.; Kong, J. Recent Progress in Detection and Profiling of Cancer Cell-Derived Exosomes. *Small* **2021**, *17*, 2007971.
(17) Pang, Y.; Shi, J.; Yang, X.; Wang, C.; Sun, Z.; Xiao, R. Personalized detection of circling exosomal PD-L1 based on Fe3O4@TiO2 isolation and SERS immunoassay. *Biosens. Bioelectron.* **2020**, *148*, 111800.
(18) Li, T. D.; Zhang, R.; Chen, H.; Huang, Z. P.; Ye, X.; Wang, H.; Deng, A. M.; Kong, J. L. An ultrasensitive polydopamine bifunctionalized SERS immunoassay for exosome-based diagnosis and classification of pancreatic cancer. *Chem. Sci.* **2018**, *9*, 5372−5382.
(19) Wang, Z.; Zong, S.; Wang, Y.; Li, N.; Li, L.; Lu, J.; Wang, Z.; Chen, B.; Cui, Y. Screening and multiple detection of cancer exosomes using an SERS-based method. *Nanoscale* **2018**, *10*, 9053−9062.
(20) Zhang, Y.; Jiao, J.; Wei, Y.; Wang, D.; Yang, C.; Xu, Z. Plasmonic Colorimetric Biosensor for Sensitive Exosome Detection via Enzyme-Induced Etching of Gold Nanobipyramid@MnO2 Nanosheet Nanostructures. *Anal. Chem.* **2020**, *92*, 15244−15252.
(21) Xu, L.; Chopdat, R.; Li, D.; Al-Jamal, K. T. Development of a simple, sensitive and selective colorimetric aptasensor for the detection of cancer-derived exosomes. *Biosens. Bioelectron.* **2020**, *169*, 112576.
(22) Zhang, Q.; Wang, F.; Zhang, H.; Zhang, Y.; Liu, M.; Liu, Y. Universal Ti3C2MXenes Based Self-Standard Ratiometric Fluorescence Resonance Energy Transfer Platform for Highly Sensitive Detection of Exosomes. *Anal. Chem.* **2018**, *90*, 12737−12744.
(23) Wang, L.; Deng, Y.; Huang, Y.; Wei, J.; Ma, J.; Li, G. Template-free multiple signal amplification for highly sensitive detection of cancer cell-derived exosomes. *Chem. Commun.* **2021**, *57*, 8508−8511.
(24) Pan, Y.; Wang, L.; Deng, Y.; Wang, M.; Peng, Y.; Yang, J.; Li, G. A simple and sensitive method for exosome detection based on steric hindrance-controlled signal amplification. *Chem. Commun.* **2020**, *56*, 13768−13771.
(25) Wang, L.; Pan, Y.; Liu, Y.; Sun, Z.; Huang, Y.; Li, J.; Yang, J.; Xiang, Y.; Li, G. Fabrication of an Aptamer-Coated Liposome Complex for the Detection and Profiling of Exosomes Based on Terminal Deoxynucleotidyl Transferase-Mediated Signal Amplification. *ACS Appl. Mater. Interfaces* **2020**, *12*, 322−329.
(26) Wang, L.; Yang, Y.; Liu, Y.; Ning, L.; Xiang, Y.; Li, G. Bridging exosome and liposome through zirconium-phosphate coordination chemistry: a new method for exosome detection. *Chem. Commun.* **2019**, *55*, 2708−2711.
(27) Xiong, H.; Huang, Z.; Lin, Q.; Yang, B.; Yan, F.; Liu, B.; Chen, H.; Kong, J. Surface Plasmon Coupling Electrochemiluminescence Immunosensor Based on Polymer Dots and AuNPs for Ultrasensitive Detection of Pancreatic Cancer Exosomes. *Anal. Chem.* **2022**, *94*, 837−846.
(28) Pan, S.; Zhang, Y.; Natalia, A.; Lim, C. Z. J.; Ho, N. R. Y.; Chowbay, B.; Loh, T. P.; Tam, J. K. C.; Shao, H. Extracellular vesicle drug occupancy enables real-time monitoring of targeted cancer therapy. *Nat. Nanotechnol.* **2021**, *16*, 734−742.
(29) Huang, R.; He, L.; Xia, Y.; Xu, H.; Liu, C.; Xie, H.; Wang, S.; Peng, L.; Liu, Y.; Liu, Y.; He, N.; Li, Z. A Sensitive Aptasensor Based on a Hemin/G-Quadruplex-Assisted Signal Amplification Strategy for Electrochemical Detection of Gastric Cancer Exosomes. *Small* **2019**, *15*, 1900735.
(30) Doldan, X.; Fagundez, P.; Cayota, A.; Laiz, J.; Tosar, J. P. Electrochemical sandwich immunosensor for determination of exosomes based on surface marker-mediated signal amplification. *Anal. Chem.* **2016**, *88*, 10466−10473.
(31) Wang, L.; Deng, Y.; Wei, J.; Huang, Y.; Wang, Z.; Li, G. Spherical nucleic acids-based cascade signal amplification for highly sensitive detection of exosomes. *Biosens. Bioelectron.* **2021**, *191*, 113465.
(32) Sun, Z.; Wang, L.; Wu, S.; Pan, Y.; Dong, Y.; Zhu, S.; Yang, J.; Yin, Y.; Li, G. An Electrochemical Biosensor Designed by Using Zr-Based Metal-Organic Frameworks for the Detection of Glioblastoma-Derived Exosomes with Practical Application. *Anal. Chem.* **2020**, *92*, 3819−3826.
(33) Wang, M.; Pan, Y.; Wu, S.; Sun, Z.; Wang, L.; Yang, J.; Yin, Y.; Li, G. Detection of colorectal cancer-derived exosomes based on covalent organic frameworks. *Biosens. Bioelectron.* **2020**, *169*, 112638.
(34) Yang, Y.; Li, C.; Shi, H.; Chen, T.; Wang, Z.; Li, G. A pH-responsive bioassay for paper-based diagnosis of exosomes via mussel-inspired surface chemistry. *Talanta* **2019**, *192*, 325−330.
(35) Tan, Y.; Sun, L.-P.; Jin, L.; Li, J.; Guan, B.-O. Microfiber Mach-Zehnder interferometer based on long period grating for sensing applications. *Opt. Express* **2013**, *21*, 154−164.
(36) Sun, L. P.; Huang, T.; Yuan, Z.; Lin, W.; Xiao, P.; Yang, M.; Ma, J.; Ran, Y.; Jin, L.; Li, J.; Guan, B. O. Ultra-high sensitivity of dual dispersion turning point taper-based Mach-Zehnder interferometer. *Opt Express* **2019**, *27*, 23103−23111.
(37) Sypabekova, M.; Korganbayev, S.; Gonzalez-Vila, A.; Caucheteur, C.; Shaimerdenova, M.; Ayupova, T.; Bekmurzayeva, A.; Vangelista, L.; Tosi, D. Functionalized etched tilted fiber Bragg grating aptasensor for label-free protein detection. *Biosens. Bioelectron.* **2019**, *146*, 111765.
(38) Zhou, L.; Liu, C.; Sun, Z.; Mao, H.; Zhang, L.; Yu, X.; Zhao, J.; Chen, X. Black phosphorus based fiber optic biosensor for

https://doi.org/10.1021/acssensors.2c00598
ACS Sens. 2022, 7, 1926−1935

ultrasensitive cancer diagnosis. *Biosens. Bioelectron.* **2019**, *137*, 140−147.
(39) Sun, D.; Sun, L.-P.; Guo, T.; Guan, B.-O. Label-free thrombin detection using a tapered fiber-optic interferometric aptasensor. *J. Lightwave Technol.* **2019**, *37*, 2756−2761.
(40) Wu, J.; Zhang, X.; Liu, B.; Zhang, H.; Song, B. Square-microfiber-integrated biosensor for label-free DNA hybridization detection. *Sens. Actuators B: Chem.* **2017**, *252*, 1125−1131.
(41) Wei, W.; Nong, J.; Zhu, Y.; Zhang, G.; Wang, N.; Luo, S.; Chen, N.; Lan, G.; Chuang, C.-J.; Huang, Y. Graphene/Au-Enhanced Plastic Clad Silica Fiber Optic Surface Plasmon Resonance Sensor. *Plasmonics* **2018**, *13*, 483−491.
(42) Wang, B.; Niu, Y.; Zheng, S.; Yin, Y.; Ding, M. An optical fiber immunosensor with a low detection limit based on plasmon coupling enhancement. *J. Lightwave Technol.* **2020**, *38*, 3781−3788.
(43) Huang, Y.; Chen, P.; Liang, H.; Xiao, A.; Zeng, S.; Guan, B.-O. Nucleic acid hybridization on a plasmonic nanointerface of optical microfiber enables ultrahigh-sensitive detection and potential photothermal therapy. *Biosens. Bioelectron.* **2020**, *156*, 112147.
(44) Xiao, A.; Huang, Y.; Zheng, J.; Chen, P.; Guan, B. O. An optical microfiber biosensor for CEACAM5 detection in serum: sensitization by a nanosphere interface. *ACS Appl. Mater. Interfaces* **2020**, *12*, 1799−1805.
(45) Li, H.; Huang, Y.; Chen, C.; Xiao, A.; Hou, G.; Huang, Y.; Feng, X.; Guan, B.-O. Real-Time Cellular Cytochrome C Monitoring through an Optical Microfiber: Enabled by a Silver-Decorated Graphene Nanointerface. *Adv. Sci.* **2018**, *5*, 1701074.
(46) Li, H.; Huang, Y.; Hou, G.; Xiao, A.; Chen, P.; Liang, H.; Huang, Y.; Zhao, X.; Liang, L.; Feng, X.; Guan, B.-O. Single-molecule detection of biomarker and localized cellular photothermal therapy using an optical microfiber with nanointerface. *Sci. Adv.* **2019**, *5*, eaax4659.
(47) Huang, Y.; Ding, M.; Guo, T.; Hu, D.; Cao, Y.; Jin, L.; Guan, B.-O. A fiber-optic sensor for neurotransmitters with ultralow concentration: near-infrared plasmonic electromagnetic field enhancement using raspberry-like meso-SiO2 nanospheres. *Nanoscale* **2017**, *9*, 14929−14936.
(48) Abid, I.; Bohloul, A.; Najmaei, S.; Avendano, C.; Liu, H. L.; Péchou, R.; Mlayah, A.; Lou, J. Resonant surface plasmon−exciton interaction in hybrid MoSe2@Au nanostructures. *Nanoscale* **2016**, *8*, 8151−8159.
(49) Liu, K.; Zhang, J.; Jiang, J.; Xu, T.; Wang, S.; Chang, P.; Zhang, Z.; Ma, J.; Liu, T. Multi-layer optical fiber surface plasmon resonance biosensor based on a sandwich structure of polydopamine-MoSe2@Au nanoparticles-polydopamine. *Biomed. Opt. Express* **2020**, *11*, 6840−6851.
(50) Liu, K.; Zhang, J.; Jiang, J.; Xu, T.; Wang, S.; Chang, P.; Zhang, Z.; Ma, J.; Liu, T. MoSe2-Au Based Sensitivity Enhanced Optical Fiber Surface Plasmon Resonance Biosensor for Detection of Goat-Anti-Rabbit IgG. *IEEE Access* **2020**, *8*, 660−668.
(51) Himbert, D.; Zeuschner, P.; Ayoubian, H.; Heinzelmann, J.; Stöckle, M.; Junker, K. Characterization of CD147, CA9, and CD70 as Tumor-Specific Markers on Extracellular Vesicles in Clear Cell Renal Cell Carcinoma. *Diagnostics* **2020**, *10*, 1034.
(52) Late, D. J.; Doneux, T.; Bougouma, M. Single-layer MoSe2 based NH3 gas sensor. *Appl. Phys. Lett.* **2014**, *105*, 233103.
(53) Patel, A. B.; Machhi, H. K.; Chauhan, P.; Narayan, S.; Dixit, V.; Soni, S. S.; Jha, P. K.; Solanki, G. K.; Patel, K. D.; Pathak, V. M. Electrophoretically Deposited MoSe2/WSe2 Heterojunction from Ultrasonically Exfoliated Nanocrystals for Enhanced Electrochemical Photoresponse. *ACS Appl. Mater. Interfaces* **2019**, *11*, 4093−4102.
(54) Wang, G.; Zhang, S.; Zhang, X.; Zhang, L.; Cheng, Y.; Fox, D.; Zhang, H.; Coleman, J. N.; Blau, W. J.; Wang, J. Tunable nonlinear refractive index of two-dimensional MoS2, WS2, and MoSe2 nanosheet dispersions. *Photon. Res.* **2015**, *3*, A51−A55.
(55) Chiavaioli, F.; Gouveia, C. A. J.; Jorge, P. A. S.; Baldini, F. Towards a uniform metrological assessment of grating-based optical fiber sensors: From refractometers to biosensors. *Biosensors* **2017**, *7*, 23.
(56) Gao, F.; Fan, T.; Wu, J.; Liu, S.; Du, Y.; Yao, Y.; Zhou, F.; Zhang, Y.; Liao, X.; Geng, D. Proximity hybridization triggered hemin/G-quadruplex formation for construction a label-free and signal-on electrochemical DNA sensor. *Biosens. Bioelectron.* **2017**, *96*, 62−67.
(57) Kim, E.; Baaske, M. D.; Vollmer, F. Towards next-generation label-free biosensors: recent advances in whispering gallery mode sensors. *Lab Chip* **2017**, *17*, 1190−1205.
(58) Liu, H. L.; Yang, T.; Chen, J. H.; Chen, H. W.; Guo, H.; Saito, R.; Li, M. Y.; Li, L. J. Temperature-dependent optical constants of monolayer MoS2, MoSe2, WS2, and WSe2: spectroscopic ellipsometry and first-principles calculations. *Sci. Rep.* **2020**, *10*, 15282.
(59) Zhu, L.; Wang, L.; Liu, Y.; Xu, D.; Fang, K.; Guo, Y. CAIX aptamer-functionalized targeted nanobubbles for ultrasound molecular imaging of various tumors. *Int. J. Nanomedicine* **2018**, *13*, 6481−6495.
(60) Cao, J.; Sun, T.; Grattan, K. T. V. Gold nanorod-based localized surface plasmon resonance biosensors: A review. *Sens. Actuators B: Chem.* **2014**, *195*, 332−351.

Recommended by ACS

Ultrasensitive Analysis of Exosomes Using a 3D Self-Assembled Nanostructured SiO_2 Microfluidic Chip
Qiaoyu Li, Shaoning Yu, *et al.*
FEBRUARY 24, 2022
ACS APPLIED MATERIALS & INTERFACES
READ

Assembly of Black Phosphorus Nanosheets and MOF to Form Functional Hybrid Thin-Film for Precise Protein Capture, Dual-Signal and Intrinsic Self-Calibration Sensi...
Yujiao Sun, Rijun Gui, *et al.*
JANUARY 06, 2020
ANALYTICAL CHEMISTRY
READ

Nanoplasmonic Sandwich Immunoassay for Tumor-Derived Exosome Detection and Exosomal PD-L1 Profiling
Chuanyu Wang, Pengyu Chen, *et al.*
SEPTEMBER 08, 2021
ACS SENSORS
READ

Surface-Functionalized Terahertz Metamaterial Biosensor Used for the Detection of Exosomes in Patients
Yao Wang, Dongxia Li, *et al.*
MARCH 17, 2022
LANGMUIR
READ

Get More Suggestions >

https://doi.org/10.1021/acssensors.2c00598
ACS Sens. 2022, 7, 1926−1935